Mathematical Biosciences and Engineering

MBE, 18(6): 7525–7538.
DOI: 10.3934/mbe.2021372
Received: 28 June 2021
Accepted: 18 August 2021
Published: 02 September 2021

http://www.aimspress.com/journal/MBE

Research article

Evaluation of rods deformation of metal lattice structure in additive manufacturing based on skeleton extraction technology

Liming Wu, Ning Dai* and Hongtao Wang*

College of Mechanical and Electrical Engineering, Nanjing University of Aeronautics and Astronautics, Nanjing 210016, China

* **Correspondence:** Email: dai_ning@nuaa.edu.cn, meehtwang@nuaa.edu.cn.

Abstract: The components with lattice structure as filling unit have great application potential in aerospace and other fields. The failure of the lattice structure directly affects the functional characteristics of the parts filled with the lattice structure. Aiming at the problem that it is difficult to evaluate the deformation degree of metal lattice structure after mechanical loading in additive manufacturing, firstly, the point cloud model of lattice structure is obtained by using CT scanning and three-dimensional reconstruction, and then the skeleton of lattice structure is automatically extracted based on L_1 median algorithm. Finally, the deformation angle of rods is measured to evaluate the degree of deformation and damage of parts. In this paper, the deformation evaluation of the rods of the BCC lattice is discussed. The experimental results show that the proposed skeleton extraction technology achieves the evaluation of lattice structure deformation. The experimental model is extended to BCC lattice structure with unit cell number of $n \times n \times n$. When the ratio of the rods with more than 40% severe deformation to all rods in the lattice structure reaches $(2n-1)/2n^2$ it indicates that the lattice structure has undergone a large degree of deformation and should not continue to serve.

Keywords: additive manufacturing; BCC lattice structure; skeleton extraction; L_1 median value; rods deformation; deformation detection

1. Introduction

Three-dimensional lattice structure is a kind of periodic porous structure, which is composed of a large number of same lattice elements. Lattice structure integrates the characteristics of lightweight, and high strength, which not only meets the load-carrying requirements, but also meets the unique

functional requirements such as heat dissipation and noise reduction. It has excellent mechanical properties and material structure function integration characteristics [1,2], therefore, the lattice structure has great application potential in aerospace and other fields [3]. Due to the complex internal structure and relatively small size of lattice structure [4,5], as well as the variety of loads and harsh service conditions, it is a challenging work to carry out quality inspection and evaluation of space complex lattice structure, especially the evaluation of rods deformation.

The domestic and foreign scholars' research on the inspection of metal lattice structure by additive manufacturing can be divided into two categories. One is the quality inspection of lattice structure after additive manufacturing, which mainly aims at surface roughness and dimensional manufacturing accuracy [6–8]. Bill et al. [9] extracted the contour and boundary information of lattice structure from CT images to analyze the roughness of its support rods. Han et al. [10] measured the surface roughness and diameter of lattice structure rods using scanning electron microscope and optical microscope. Xiao et al. [11] analyzed the error of two lattice units with different topological configurations by matching the 3D model reconstructed by CT scanning with its design model, and analyzed the error value after the matching. The other is to evaluate the quality of lattice structure after the load is applied, which mainly focuses on the failure behavior of lattice rods such as fracture. Hamza et al. [12] used industrial CT to detect the three-dimensional shape of lattice structure before and after stretching, and collected two-dimensional images, then characterized the failure behavior of lattice structure fracture rod by electron microscope, and studied the morphology characteristics of lattice structure by optical microscope.

The lattice structure can be simplified into a skeleton model, and the skeleton of the lattice structure can be obtained by using the skeleton extraction technology to evaluate the deformation of the lattice structure. The studies on skeleton extraction are roughly divided into two categories. One is grid-based skeleton extraction. These algorithms are designed for sealed surface mesh models without missing holes. Au et al. [13] proposed the Laplacian shrinkage method, which shrinks the mesh to the middle of the model by constantly balancing the shrinking and pulling energies. Tagliasacchi et al. [14] proposed similar improvements based on Mean Curvature Flow. This type of method is concise, easy to understand, and highly robust. The other is based on point cloud skeleton extraction. Tagliasacchi et al. [15] proposed the ROSA method, which assumes that the local basic shape and structure of the object model is a cylinder, and uses the normal vector information to calculate an optimal tangent plane for each point on the point cloud to fit an ellipse, and finally Connect the central axis points of all tangent planes to form a curved skeleton. Huang et al. [16] applied the median theory locally on the point cloud model to obtain the local center point set, and cleverly added the repulsion term to form a continuous one-dimensional space structure. Hu et al. [17] extracts the cross-section centroid set of the point cloud model and connects them to form a main connection curve skeleton. At present, the study on the lattice structure is still in its infancy. Due to the complex internal structure of the lattice structure, it is difficult to detect the deformation of the rods after being stressed by the existing equipment. There are few studies on the deformation degree detection of the rods in the lattice structure after loading. In this paper, based on the geometric skeleton extraction technology of lattice structure, the deformation evaluation of additive manufacturing metal lattice structure after loading is carried out.

2. Detailed technical route

There are a large number of lattice elements in lattice structure, and the scale of 3D reconstruction model data is huge, which makes the calculation load heavy in the actual processing process.

Therefore, it is necessary to simplify the data on the basis of representing the characteristic information of the 3D model as complete as possible. Skeleton line is an effective form to describe the topological structure of objects, which provides a more intuitive definition for model representation and geometric feature recognition. It can not only retain feature information to the greatest extent, but also reduce the difficulty of algorithm operation [18]. In this paper, a lattice structure skeleton extraction algorithm based on L_1 median is proposed. The skeleton model is used to represent the topological shape of lattice structure, and finally the deformation evaluation of lattice structure is realized through the skeleton model.

The lattice structure to which this method is applicable is shown in Figure 1. In order to reduce the amount of calculation in the process of model processing, its topological configuration is simplified as "nodes" and "skeleton lines". "Skeleton lines" are the central axis of the lattice element rods (represented by the number in Figure 1), "nodes" are the intersection points of multiple skeleton lines (represented by the letter in Figure 1). In this paper, the deformation evaluation of the rods of the body centered cubic (BCC) lattice is discussed.

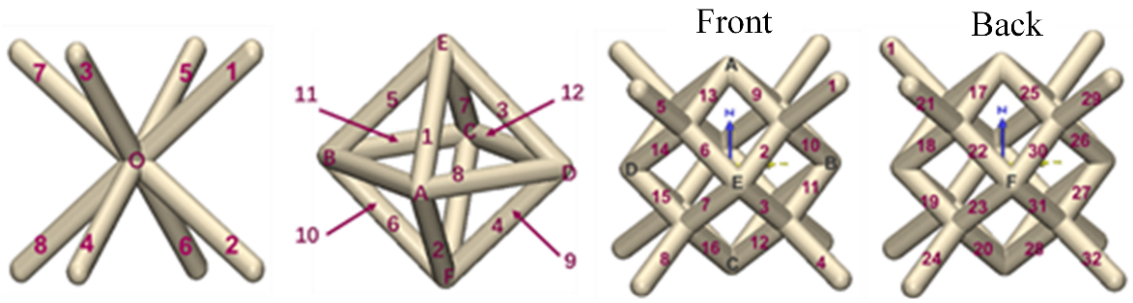

Figure 1. Common lattice structure. (a) Body-centered cubic (BCC); (b) Regular octahedral cell (OCT); (c) Dodecahedral unit cell (DOD).

The technical route of deformation assessment of metal BCC lattice structure rods made by additive manufacturing is shown in Figure 2. Firstly, the lattice structure is preprocessed, which includes loading the lattice structure to obtain the deformed lattice structure, CT scanning it to obtain the two-dimensional image sequence, and the image sequence is reconstructed to obtain the three-dimensional lattice model after mechanical loading; then, based on L_1 median algorithm, skeleton points in the center of lattice structure are extracted, and a series of skeleton points are fitted and extended to obtain the complete geometric skeleton of lattice structure; finally, since the lattice structure rods made of titanium alloy and aluminum alloy are still linear after deformation, the degree of deformation of each rod and the overall deformation of the lattice structure can be evaluated by calculating the angle between the rods.

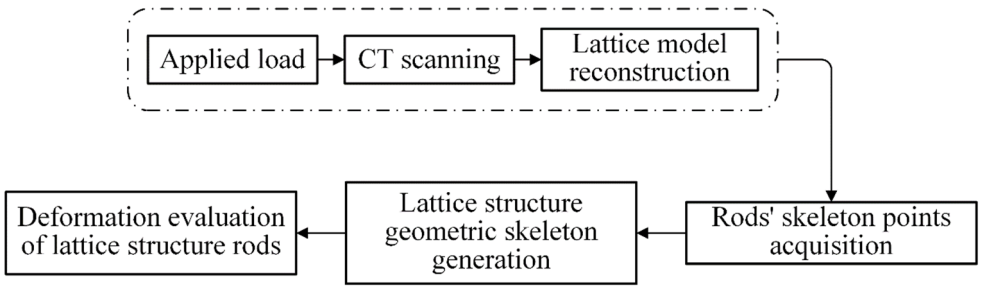

Figure 2. Technical route for deformation assessment of metal lattice structure members fabricated with additive materials.

3. Extraction of skeleton of lattice structure

3.1. Skeleton points extraction of lattice structure rods based on L_1 median

The definition of L_1 median value is shown in Eq (1), that is, x is the point with the smallest sum of distances to all points in a given set of points. Where $O=\{o_j\}_{j\in J}\subset \mathrm{R}^3$ is the set of given points and $X=\{x\}\subset \mathrm{R}^3$ is the final global L_1 median point.

$$x=\operatorname{argmmin}\sum_{j\in J}\|x-o_j\| \tag{1}$$

Daszykowski [19] proved that the median value of L_1 is the unique global center of a given set of points, but it cannot form the skeleton line of the lattice structure. Therefore, the local L_1 median value is introduced. A sampling point x only considers the original points in its neighborhood, and all the original points whose distance from x is less than the threshold value are regarded as the adjacent original points of x, forming the original point neighborhood of x. The revised definition of L_1 median is shown in Eq (2):

$$\operatorname*{argmmin}_{x}\sum_{i\in I}\sum_{j\in J}\|x_i-o_j\|\theta(\|x_i-o_j\|) \tag{2}$$

Where $O=\{o_j\}_{j\in J}\subset \mathrm{R}^3$ is the input point set, $X=\{x_i\}_{i\in I}\subset \mathrm{R}^3$ is the point set obtained by random down sampling from O, and the number of points $|I|=|J|$. $\theta(r)$ is a Gaussian weight function, and the specific expression is shown in Eq (3):

$$\theta(r)=e^{-r^2/(h/2)^2} \tag{3}$$

Where r is the distance between the sampling point x_i and the original point o_j, and h is the parameter used to control the neighborhood size. The closer the original point o_j is to x_i, the greater the weight is; the farther away the original point o_j is from x_i, the smaller the weight is. The iterative solution of local L_1 median is:

$$x^*=\sum_{j\in J}\frac{o_j\omega_j^{'}}{\sum_{j\in J}\omega_j^{'}} \tag{4}$$

Where $\omega_j^{'}$ is the weight function and $\omega_j^{'}=\theta(\|x^*-o_j\|)$.

Skeleton lines are extracted based on L_1 median algorithm, and the sample points are iteratively contracted by expanding the neighborhood radius to form skeleton points. Generally, the distribution of points in three-dimensional space is described by the degree of dispersion or density. In the branch position of skeleton, the distribution of points is relatively scattered. In the main part of skeleton, the points are relatively concentrated on one-dimensional line. In this case, covariance matrix is needed to describe the dispersion of sampling points. For any sampling point x_i, the covariance matrix is as follows:

$$C_i = \sum_{i' \in I \setminus \{i\}} \theta(\| x_i - x_{i'} \|)(x_i - x_{i'})^{\mathrm{T}}(x_i - x_{i'}) \tag{5}$$

Where x_i is the row vector, C_i is a 3×3 matrix, and $x_{i'}$ is the row vector at any point except x_i in the sampling point set X. The three eigenvalues of the matrix are $\lambda_i^0 \le \lambda_i^1 \le \lambda_i^2$ and the corresponding three eigenvectors $\{v_i^0, v_i^1, v_i^2\}$, which represent the three main directions of the point distribution. The eigenvalue represents the density of the points in the direction. The larger the eigenvalue is, the denser the points in this direction are. On the contrary, the more scattered the points are. The distribution measure is defined to describe the distribution of points:

$$\sigma_i = \sigma(x_i) = \frac{\lambda_i^2}{\lambda_i^0 + \lambda_i^1 + \lambda_i^2} \tag{6}$$

Based on the description of point distribution metric in Eq (6), the definition of regular term of point distribution metric can be obtained, that is $R(X)$:

$$R(X) = \sum_{i \in I} \gamma_i \sum_{i' \in I \setminus \{i\}} \frac{\theta(\| x_i - x_{i'} \|)}{\sigma_i \| x_i - x_{i'} \|} \tag{7}$$

Where $\{\gamma_i\}_{i \in I}$ is the equilibrium parameter, which makes the gravitational force of the input points and the repulsive force of the sampling points balance. Finally, the final definition of L_1 median algorithm is shown in Eq (8):

$$\underset{x}{\operatorname{argmin}} \sum_{i \in I} \sum_{j \in J} \| x_i - o_j \| \theta(\| x_i - o_j \|) + R(X) \tag{8}$$

Among them, the first term $\underset{x}{\operatorname{argmin}} \sum_{i \in I} \sum_{j \in J} \| x_i - o_j \| \theta(\| x_i - o_j \|)$ is the local L_1 median, and the second term $R(X)$ is the regular term. By solving Eq (8), the set of iterative points can be obtained:

$$x_i^{k+1} = \frac{\sum_{j \in J} o_j \alpha_{ij}^{\ k}}{\sum_{j \in J} \alpha_{ij}^{\ k}} + \mu \sigma_i^{\ k} \frac{\sum_{i' \in I \setminus \{i\}} (x_i^{\ k} - x_{i'}^{\ k}) \beta_{ii'}^{\ k}}{\sum_{i' \in I \setminus \{i\}} \beta_{ii'}^{\ k}} \tag{9}$$

Where $\alpha_{ij}^{\ k} = \frac{\theta(\| x_i^{\ k} - o_j \|)}{\| x_i^{\ k} - o_j \|} (j \in J)$, $\beta_{ii'}^{\ k} = \frac{\theta(\| x_i^{\ k} - x_{i'}^{\ k} \|)}{\| x_i^{\ k} - x_{i'}^{\ k} \|^2} (i' \in I \setminus \{i\})$, $\sigma_i^{\ k} = \sigma(x_i^{\ k})$, μ is the parameter controlling the repulsion force between sampling points, and $\mu \in [0, 0.5)$. In this paper, $\mu = 0.33$.

After solving Eq (8), X becomes regular, that is, the central skeleton points of the point cloud.

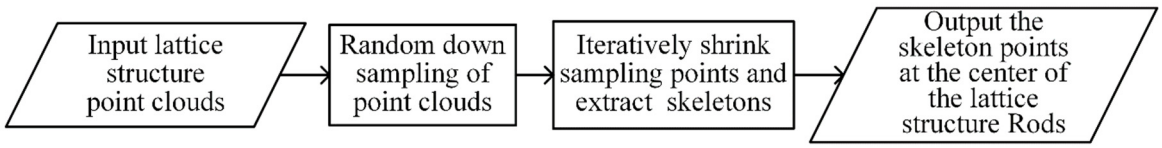

Figure 3. L_1 median algorithm.

According to the L_1 median theory, the extraction process of BCC lattice structure rods skeleton points is shown in Figure 3, in which the main steps are random down sampling of point cloud and iterative shrinkage of sampling points. Random down sampling of point cloud is very important for skeleton point extraction. In this paper, the classical shuffling algorithm is used for down sampling. The more the number of sampling points is, the more accurate the result is, and the corresponding amount of calculation will also increase, thus greatly prolonging the running time of the program; the less the number of samples, the less the amount of calculation, but the accuracy of the extracted skeleton line will also decline. Therefore, it is necessary to select an appropriate number of samples and define the sampling rate as:

$$\alpha = \frac{n_{sam}}{n_{org}} \tag{10}$$

Where n_{sam} is the number of sampling points and n_{org} is the number of points in the input point cloud.

In the iterative contraction process of sampling points, it is necessary to obtain the "gravitation" and "repulsion" of sampling points, that is, the first and second terms of Eq (8): The solution of "gravity" needs to be determined by the neighborhood of each sampling point in the input point set, and the L_1 local median value of the sampling point can be obtained; "The solution of "repulsive force" needs to be determined according to other sampling points in the neighborhood of each sampling point, and the regularization term with point distribution can be obtained.

The specific steps of extracting skeleton points of lattice structure rods are as follows:

(a) Random down sampling of the original point clouds set J to get the point set I;

(b) According to the neighborhood radius h, the neighbor set N_{org} in J and the neighbor set N_{sam} in I of each sampling point x_i are calculated;

(c) According to Eq (5), σ_i of each point x_i is calculated;

(d) Traverse each x_i in I:

① Traverse every adjacent point $x_{i'}$ of x_i in N_{sam}, calculate the right term of Eq (8), and get the three-dimensional vector repulsion;

② Traverse every adjacent point o_j of x_i in N_{org}, calculate the left term of Eq (8), and get the three-dimensional vector average;

(e) In I, $x_i = \text{average}_i + \sigma_i \cdot \mu \cdot \text{repulsion}_i$;

(f) If the change between the two iterations is greater than the set value, or the neighborhood radius reaches the preset threshold, the iteration ends.

Figure 4 shows the effect of extracting skeleton points of $3\times3\times1$ BCC lattice structure at different sampling rates. When α is 3%, the extracted skeleton points are incomplete. When α is 5% or 10%, the extracted skeleton points are complete, and the effect is not obvious in the two cases.

Therefore, the sampling rate α is finally selected as 5%.

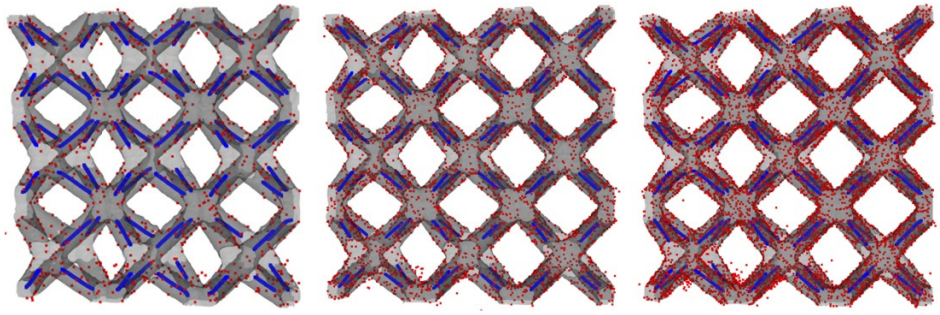

(a) (b) (c)

Figure 4. The sampling rate of skeleton points. (a) $\alpha = 3\%$; (b) $\alpha = 5\%$; (c) $\alpha = 10\%$.

3.2. Generation of geometric framework of lattice structure

Considering the particularity of the lattice structure, the rods are still a cylinder without deformation, but they are broken at the cross nodes of the rods. Therefore, it is only necessary to calculate the local L_1 median points in the middle of the rod, and fit these points with a straight line to get the current central axis of each rod. After that, extend the central axis of each rod, and the extension intersection of the central axis of the rod without fracture is the "node" (i.e., point O in Figure 5(a)). By searching the central axis of the rod near the node O, the fracture position can be obtained. By associating the central axis of the rod with node O, the central axis of all rods in the unit cell with O as the center point can be found. Thus, the angle deformation of the rods of each unit cell is measured after mechanical loading.

The specific steps of skeleton points optimization are as follows:

(a) The extracted skeleton points are fitted as straight lines, and the direction vector set L of the straight line and the point set P composed of a point on the straight line are obtained;

(b) According to the point P_i in the point set P, all the points are sorted according to the coordinates, and the position of each rod relative to the center point of each unit cell is obtained;

(c) The center point set C of a unit cell is obtained by intersection of the center lines of every eight rods. The initial value C_O of the center point is obtained by average value of the center point set C. If the distance between the intersection of the center lines of the two rods and C_O is greater than a certain threshold, the point will be deleted. The corresponding rod of the point will be defined as a severely deformed rod, and the center point C_O of C will be obtained again, This process is repeated until the distance from all intersections to C_O is less than the threshold;

(d) The center point of each cell and the direction vector of each rod are known. For the severely deformed rod, a straight line of specified length is drawn from the center point along the direction vector, and finally the skeleton lines of the lattice structure are obtained.

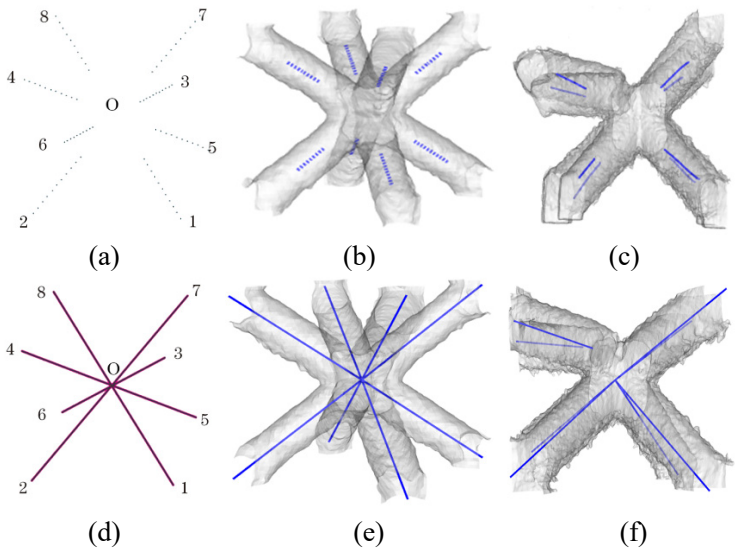

Figure 5. Generation of geometric skeleton of unit cell feature. (a) The "skeleton points" of the rods; (b) The "skeleton points" are extracted from the undeformed cell; (c) The "skeleton points" are extracted from the deformable cell; (d) Fitting line with the "Skeleton points"; (e) The undeformed cell generates a complete skeleton line; (f) After deformation, the unit cell generates complete skeleton lines.

3.3. Deformation evaluation of lattice rods

When the uniformly distributed load is applied, the rods of lattice structure deform and fracture along the direction of force. Therefore, the deformation degree of the rods after mechanical loading of lattice structure is mainly obtained by detecting the angle change of the rods in the direction of force in each unit cell. As shown in Figure 6, the selected lattice unit is defined as L_1 layer, L_2 layer and L_3 layer from top to bottom. The number of lattice cells in each layer is $3\times1\times1$, which is defined as cell $L_{mn}\,(m,n=1,2,3)$ from left to right. The angles of rods 1 and 3, 2 and 4, 5 and 7, 6 and 8 in each unit cell are measured. The direction vector of each rod is recorded as V, and the measured angle is recorded as $\theta_{ij}\,(i=1,2,5,6,\ j=3,4,7,8)$. In BCC standard model, the design value of θ_{ij} is 70.5°.

By multiplying the space vectors V_i and V_j of the two rods on the unit cell, the space angle θ_{ij} of the two rods is obtained:

$$\cos\theta_{ij}=\frac{V_i\cdot V_j}{|V_i|*|V_j|} \tag{11}$$

After obtaining the required angles θ_{ij}, it is consistent with the design value of 70.5°. According to the change range of θ_{ij}, the deformation of lattice structure is evaluated.

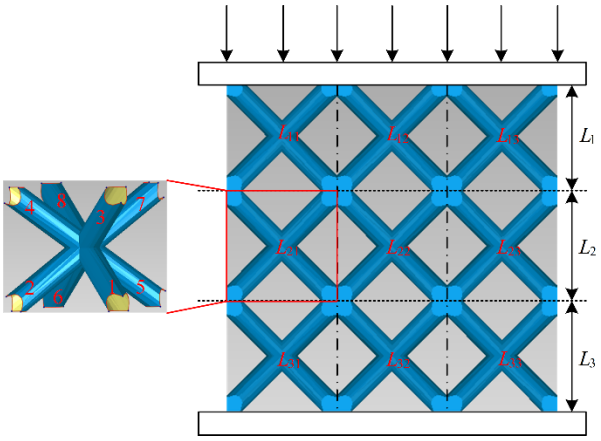

Figure 6. Lattice structure deformation model.

4. Experimental results and discussion

4.1. Lattice structure preprocessing

In this paper, BCC lattice model is used as the experimental object, the rod diameter is 2 mm, the material is titanium alloy Ti6Al4V, the size is 30 mm×30 mm×30 mm, the number of cells is $3\times3\times3$, the selective laser melting manufacturing process is adopted, the equipment is EOS M400, the laser power is 280 W, the layer thickness is 30μm, the scanning speed is 1200 mm/s and the width of printing room is 0.14 mm.

The preprocessing of lattice structure are as follows:

(1) Firstly, the quasi-static compression experiment of BCC lattice model is carried out. The experimental method refers to GB/T 7314-2017 "metallic materials room temperature compression experimental method", and the unidirectional compression experiment is carried out on the experimental sample by using electronic universal material testing machine. The experimental equipment is electronic universal material testing machine, the manufacturer is HUALONG, and the model is WDW. If the lattice has deformation, that is, when the lattice structure is completely broken into several parts, there is no need to carry out the rods' deformation detection. Therefore, when it is observed that only part of the rods of lattice structure fracture, but the lattice structure doesn't have plastic deformation, the experiment is stopped.

Table 1. CT scanning parameters of lattice structure.

Parameters	Value
Scan Voltage /kV	420
Scan Current /mA	1.6
Integration time /ms	250
Magnification	2.1
Voxel size / m	200
Gain	0.25
Pre-filter	1.5 mm Cu

(2) The lattice model after mechanical loading is scanned by CT, and the scanning equipment is IPT04103D. The scanning parameters are shown in Table 1. After CT scanning, the sequence images of lattice structure can be obtained, and the mesh model or point cloud model of lattice structure after mechanical loading can be reconstructed by using marching cube algorithm, namely STL, PLY, OBJ and other formats, and then skeleton lines can be extracted from the generated model.

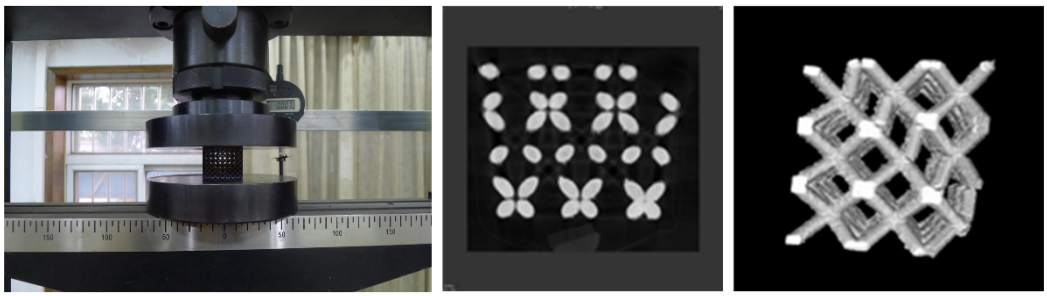

(a) (b) (c)

Figure 7. Lattice structure preprocessing. (a) Lattice quasi-static compression experiment; (b) Sequence images after CT scanning; (c) 3D model of lattice structure after image reconstruction.

4.2. Extraction of lattice structure skeleton

The BCC lattice model selected in this experiment is shown in Figure 8(a), and the lattice model after pressure loading is shown in Figure 8(b). According to Figure 8(b), in the direction of force loading, the deformation of the three-layer lattice structure from front to back is basically the same. In order to improve the detection efficiency and reduce the computing load of the computer, only $3\times3\times1$ lattice units are intercepted for analysis. The intercepted part is shown in Figure 9(a). The L_1 median algorithm described in this paper is used to extract the skeleton lines. The effect after the completion of the algorithm is shown in Figure 9(b). After the optimization of the skeleton points in the center of the lattice structure rods, the complete skeleton lines of the lattice structure after mechanical loading is obtained, as shown in Figure 9(c).

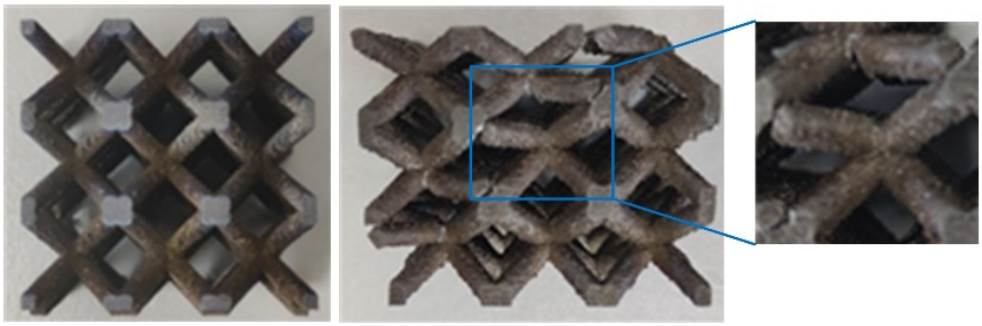

(a) (b)

Figure 8. BCC lattice model. (a) Original lattice structure; (b) Lattice structure after pressure loading.

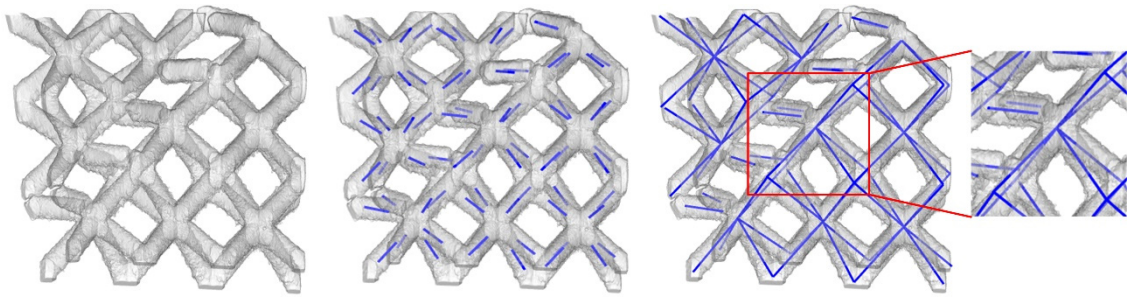

(a) (b) (c)

Figure 9. Lattice structure skeleton extraction. (a) Selected lattice units; (b) Extraction of skeleton points in the center of rods based on lattice structure; (c) Complete skeleton lines of lattice structure after mechanical loading (the scale is 1:1.3).

The results of using the skeleton lines extraction algorithm based on the L_1 median value proposed in this paper to detect the angles of the first to third layer rods after mechanical loading are shown in Table 2 (Note: "–" in the table means that the rods fail after mechanical loading, and the angle cannot be measured). The line chart according to the angle of the unit cell rods of each layer in the selected area is shown in Figure 10.

Table 2. Rods angle values of each layer unit cell.

Area \ Angle		θ_{13} /°	θ_{24} /°	θ_{57} /°	θ_{68} /°
L_1	L_{11}	51.6743	55.6354	52.1447	53.7984
	L_{12}	28.5991	53.6314	25.5919	51.4421
	L_{13}	–	31.0739	33.0057	–
L_2	L_{21}	37.4437	61.6417	60.6833	38.1351
	L_{22}	58.6888	35.7548	37.3582	58.951
	L_{23}	60.9467	59.3037	61.4736	62.0309
L_3	L_{31}	70.1933	38.9724	38.9211	67.3446
	L_{32}	68.5487	66.999	68.0281	67.9142
	L_{33}	66.3276	66.8002	67.6431	66.6511

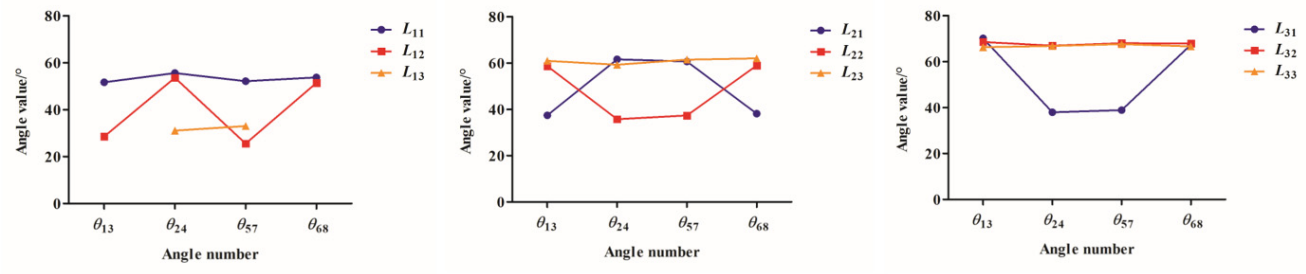

(a) (b) (c)

Figure 10. Angle change of each layer of cell rods in selected area. (a) The angle value of each unit cell rods in L_1 layer; (b) The angle value of each unit cell rods in L_2 layer; (c) The angle value of each unit cell rods in L_3 layer.

4.3. Analysis and discussion

According to the data in Table 2 and Figure 10: (1) Compared with the design model rods angle of 70.5°, the angles of the L_1 layer at the break of the rods are between 25° and 35°, and the range of change is the largest, followed by the L_2 layer (35°–38°), the angles of the L_3 layer have the smallest degree of change (38°–40°); (2) The angles of L_1 layer are the largest at the position where the rods are not broken but deformed, and the angle of each rod is between 50° and 55°, followed by the L_2 layer (58°–62°), the angles of the L_3 layer have the smallest degree of change (66°–70°).

Taking the $3\times3\times3$ BCC lattice structure of the experimental object in this paper as an example, the angle range and failure ratio of the rods when the lattice structure deforms and fails can be obtained. When the measured angle θ_{ij} of the two rods is between 20° and 40°, that is, more than 40% ($(70.5-40)/70.5*100\%=42.5\%$) deformation occurs relative to the design angle of 70.5°, indicating that the lattice structure is seriously deformed along the oblique section from the upper left to the lower right, or the rods is broken. This kind of lattice structure is about to fail. By analyzing the data in Table 2 and Figure 10, the failure rate of the $n\times n\times n$ lattice structure is defined as:

$$f(n)=\frac{m}{4n^2} \tag{12}$$

Where m is the number of rod angles less than 40° in the $n\times n\times n$ lattice structure, $4n^2$ is the total number of measured angles. In $4n^2$, n^2 is the number of unit cells of $n\times n\times1$, 4 is 4 angles are measured for each unit cell.

More than 10 of the 36 angles measured by the model in this paper are less than 40°, and the failure rate is 10/36. The mechanical properties of the BCC lattice structure are basically the same, which can be extended to $2\times2\times2$, $4\times4\times4$ lattice structure. When it is measured that failure rate of the rods is 6/16, 14/64 or greater than this ratio, it means that the lattice is about to fail. This conclusion can be generalized to the $n\times n\times n$ lattice structure, and m can be summarized as $2\times(2n-1)$. Therefore, the final expression for the failure rate $f(n)$ is:

$$f(n)=\frac{2\times(2n-1)}{4n^2}=\frac{(2n-1)}{2n^2} \tag{13}$$

When the rods are severely deformed by more than 40% and the failure rate reaches $(2n-1)/2n^2$, it indicates that the rods of the lattice structure have undergone a large degree of deformation along the oblique section from the upper left to the lower right, and the structure is about to fail.

5. Conclusions

In this paper, based on the L_1 median lattice structure skeleton extraction technology, the deformation evaluation of the BCC lattice structure is realized, and the conclusions are as follows through experiments:

1) Based on the L_1 median algorithm, it can effectively extract the "skeleton point" of the center of the lattice structure after mechanical loading. On this basis, the geometric skeleton can be generated to obtain the deformation degree of the rods and evaluate the overall deformation of the lattice structure;

2) For a BCC lattice structure with a unit cell number of $n\times n\times n$, when the ratio of the rods with more than 40% severe deformation to all rods in the lattice structure reaches $(2n-1)/2n^2$, it indicates

that the rods of the lattice structure have undergone a large degree of deformation along the oblique section from the upper left to the lower right, and this structure is about to fail;

3) The method proposed in this paper is suitable for lattice structure with large deformation or partial fracture.

Acknowledgments

This study was financially supported by the National Natural Science Foundation of China (No. 51775273), Aeronautical Science Foundation of China (No. 2020Z049052002), National Defense Basic Scientific Research Program of China (No. JCKY2018605C010) and Jiangsu Province Science and Technology Support Plan Project (No.BE2018010-2).

Conflict of interest

The authors declare that there is no conflict of interests regarding the publication of this paper.

References

1. H. Chen, Q. Wu, A review of porous structure modeling of bone scaffolds, *Mod. Manuf. Eng.*, **6** (2019), 147–153.
2. Y. Tang, G. Dong, Q. Zhou, Y. Zhao, Lattice structure design and optimization with additive manufacturing constraints, *IEEE Trans. Autom. Sci. Eng.*, **15**(2017), 1546–1562.
3. A. Singh, V. Chandrasekar, P. Janapareddy, D. Mathews, P. Laux, A. Luch, et al., Emerging application of nanorobotics and artificial intelligence to cross the BBB: advances in design, controlled maneuvering, and targeting of the barriers, *ACS Chem. Neurosci.*, **12** (2021), 1835–1853.
4. C. Yi, L. Bai, X. Chen, F. Liu, J. Zhang, Z. Long, Overview of the research and application status of metal three-dimensional lattice structure topology, *Funct. Mater.*, **48** (2017), 10055–10065.
5. C. Peng, S. Cen, C. Chen, B. Zhang, Y. Hu, Research progress of carbon fiber resin matrix composite lattice and its molding process, *Fiber Compos. Mater.*, **34** (2017), 17–27.
6. L. Bai, F. Xiong, X. Chen, C. Yi, J. Zhang, R. Chen, Research on multi-objective structural optimization design of Ti6Al4V lightweight lattice structure prepared by SLM, *Chi. J. Mech. Eng.*, **54** (2018), 156–165.
7. S. Su, N. Dai, X. Cheng, L. Ding, Lattice structure size measurement based on skeleton template feature matching, *Mech. Design Manuf. Eng.*, **50** (2021), 5–10.
8. A. Singh, M. Ansari, S. Wang, P. Laux, A. Luch, A. Kumar, et al., The Adoption of Three-Dimensional Additive Manufacturing from Biomedical Material Design to 3D Organ Printing, *Appl. Sci.*, **9** (2019), 811:1–811:13.
9. B. Lozanovski, M. Leary, P. Tran, D. Shidid, M. Qian, P. Choong, Computational modelling of strut defects in SLM manufactured lattice structures, *Mater.Design*, **171** (2019), 107671.
10. X. Han, H. Zhu, X. Nie, G. Wang, X. Zeng, Investigation on selective laser melting AlSi10Mg cellular lattice strut: Molten pool morphology, surface roughness and dimensional accuracy, *Materials*, **11** (2018), 1–13.
11. Z. Xiao, Y. Yang, R. Xiao, Y. Bai, C. Song, D. Wang, Evaluation of topology-optimized lattice structures manufactured via selective laser melting, *Mater. Design*, **143** (2018), 27–37.

12. H. Alsalla, L. Hao, C. Smith, Fracture toughness and tensile strength of 316L stainless steel cellular lattice structures manufactured using the selective laser melting technique, *Mater. Scie. Eng.*, **669** (2016), 1–6.
13. O. Au, C. Tai, H. Chu, D Cohen-Or, T. Lee, Skeleton extraction by mesh contraction, *ACM Trans. Graphics*, **27** (2008), 44:1–44:9.
14. A. Tagliasacchi, I. Alhashim, M. Olson, H. Zhang, Mean curvature skeletons, *Comput. Graphics Forum*, **31** (2012), 1735–1744.
15. A. Tagliasacchi, H. Zhang, D. Cohen-Or, Curve skeleton extraction from incomplete point cloud, *ACM Trans. Graphics*, **28** (2009), 71:1–71:9.
16. H. Huang, S. Wu, D. Cohen-Or, M. Gong, H. Zhang, G. Li, et al., L-1-Medial Skeleton of Point Cloud, *ACM Trans.Graphics*, **32** (2013), 65:1–65:8.
17. H. Hu, Z. Li, X. Jin, Z. Deng, M. Chen, Y. Shen, Curve Skeleton Extraction from 3D Point Clouds Through Hybrid Feature Point Shifting and Clustering, *Comput. Graphics Forum*, **39** (2020), 111–132.
18. N. Takano, H. Takizawa, P. Wen, K. Odaka, S. Matsunaga, S. Abe, Stochastic prediction of apparent compressive stiffness of selective laser sintered lattice structure with geometrical imperfection and uncertainty in material property, *Int. J. Mech. Sci.*, **134** (2017), 347–356.
19. M. Daszykowski, K. Kaczmarek, Y. Heyden, B. Walczak, Robust statistics in data analysis - a review: basic concept, *Chemom. Intell. Lab. Syst.*, **85** (2007), 203–219.

AIMS Press